Int. Journ. of Unconventional Computing, Vol. 1, pp. 123–147
Reprints available directly from the publisher
Photocopying permitted by license only

© 2005 Old City Publishing, Inc.
Published by license under the OCP Science imprint,
a member of the Old City Publishing Group

Analog Reaction-Diffusion Chip Imitating Belousov-Zhabotinsky Reaction with Hardware Oregonator Model

TETSUYA ASAI*, YUSUKE KANAZAWA, TETSUYA HIROSE AND YOSHIHITO AMEMIYA

Graduate School of Information Science and Technology, Hokkaido University, Kita 13, Nishi 8, Kita-Ku, Sapporo 060-8628, Japan.

Recevied 5 June 2004; Accepted 18 June 2004

We introduce analog integrated circuits that imitate a typical model of a reaction diffusion system, called the Belousov-Zhabotinsky (BZ) reaction. The BZ reaction gives us many insights into developing new architectures based on a new computing paradigm such as in active wave computing. The analog unit circuit exhibits both excitatory and oscillatory behaviors with very stiff responses, as observed in typical BZ reactions. Spatiotemporal behaviors of an array of unit circuits, including synchronization of cell circuits and production of traveling waves, are demonstrated through both circuit simulation and experiments on the fabricated chip.

Keywords: reaction-diffusion system, Oregonator, analog VLSI, cellular automata

1. INTRODUCTION

Nonlinear oscillatory phenomena can be observed everywhere in the world. For instance, dissipative and autocatalytic reaction systems, which include almost every natural phenomenon, produce various spatiotemporal patterns through oscillatory reactions andthe diffusion of chemical species. Chemical systems where the reaction and diffusion of chemical species coexist under a nonequilibrium condition are called reaction-diffusion (RD) systems [27]. Typical oscillatory behavior in RD

* E-mail: asai@sapiens-ei.eng.hokudai.ac.jp

systems can be observed in the Belousov-Zhabotinsky (BZ) reaction, which is a periodic oxidation-reduction phenomenon in liquid-state reagents. It produces a variety of rhythms and orders in the form of propagating chemical waves [15].

The RD system gives us important clues into the relation between chemical reactions and vital natural phenomena. Recent topics in this field have concerned the control of phase-lagged stable synchronous patterns in two-dimensional (2D) space, called modelock or spiral waves [23,35]. Modelock is normally a negative factor in artificial systems because of the difficulty of controlling, and thus predicting, its dynamic behavior. It hampers the desired in-phase synchronization of oscillator arrays, e.g., generating an irregular heartbeat or unpredictable skews in a 2D array of voltage-controlled oscillators for VLSI clocking. Several ideas for practical applications that use the properties of RD systems have also been proposed, e.g., ideas for chemical image processing [5,21,30,32], pattern recognition [5,12,18–20,40], path planning [3,7,31,33], robot navigation [6] , and many more (see overview in Adamatzky [2001]). The computational universality of RD chemical media was demonstrated in a series of work in implementing logical gates and diodes in excitable (BZ system) [11,18,19,24–26,33,38] and non-excitable [4] chemical media; and, possible implementation of memory units in a BZ medium was discussed by Motoike *et al.* [2001]. These results suggest that natural systems that make actions primarily for themselves will help us both understand RD systems and reconstruct them in artificial reaction media.

RD phenomena are usually observed in liquid-, gel- or gas-state media. Our primary interest was to construct an artificial RD system on *solid-state media*, and to develop practical applications using the solid-state RD system that could cope easily with conventional digital computers. Our group is developing this artificial RD system, which we call a *reaction-diffusion chip*, to imitate various natural RD phenomena (e.g., orders and rhythms, pattern formation, and self organization in biological systems) on silicon VLSIs [9,10,14,28].

Implementing RD systems in hardware (VLSI) has several advantages. Hardware RD systems are very useful in simulating RD phenomena, even if the phenomena never occur in nature. This implies that a hardware system is a possible candidate for developing an artificial RD system that is superior to a natural system. For instance, hardware RD systems can operate at much faster speeds than actual RD systems. The

velocity of chemical waves in a BZ reaction is $O(10^{-2})$ m/s [37], while that of a hardware RD system will be over a million times faster than that of the BZ reaction, independent of system size [9,10]. This property is useful for developers of RD applications because every RD application benefits from high speed operations. These properties encouraged us to develop these RD chips.

The RD system can be implemented on VLSIs in terms of cellular automaton (CA) [9]. Each cell represents a spatial point in RD space. Although digital circuits are useful for controlling nonlinearities in these cells, the cell circuitoccupies a large area on a VLSI [9]. Device-level implementation of a cell, on the other hand, where nonlinearity of the cell is controlled by the physical properties of semiconductor devices rather than electrical circuits, resultsin the development of large-scale RD systems. However, controlling the cell's properties is very difficult after the device is fabricated (e.g., [10]). In this paper, we introduce CMOS RD circuits based on analog CA that are aimed at i) large-scale implementation of cells compared with digital RD circuits, and ii) easy control of cell properties. This paper is organized as follows. Section 2 outlines an RD system. Then, in Sec. 3, after introducing conventional CA models for the BZ reaction, an analog CA model is introduced. Section 4 presents circuit structures for the analog CA. Dynamic behaviors of the CA circuit are discussed in Sec. 5. Section 6 summarizes the paper.

2. REACTION-DIFFUSION MODELING

Chemical reactions are formulated in terms of temporal differences in the concentration of chemical species. For example, if substance x is dissolved in water, the temporal difference in the concentration of x is expressed, by an ordinary differential equation (ODE), as

$$\frac{d[x]}{dt} = -k[x], \tag{1}$$

where $[x]$ represents the concentration and k the rate constant. Although Eq. (1) is a linear ODE, most chemical reactions, including dissipative and autocatalytic reactions in natural systems, will be formulated by nonlinear ODEs with theright side of Eq. (1) represented by a polynomial of $[x]$. Nonlinear chemical reactions with multiple chemical species are thus represented by a set of nonlinear ODEs as

$$\frac{d[x_i]}{dt} = f_i([x_1],[x_2],\ldots,[x_N]), (i = 1,2,\ldots,N), \tag{2}$$

where N is the number of species and f_i represents the nonlinear reactive functions that depend on several different reactive species x_i.

The Belousov-Zhabotinsky (BZ) reaction was formulated as Eq. (2). One well known model of the BZ reaction is referred to as the two-variable Oregonator [27]. The dynamics are given by

$$\frac{d[x_1]}{dt} = \frac{1}{\tau}([x_1](1-[x_1]) - a[x_2]\frac{[x_1]-b}{b+[x_1]}), \tag{3}$$

$$\frac{d[x_2]}{dt} = [x_1]-[x_2], \tag{4}$$

where $[x_1]$ and $[x_2]$ represent the abridged concentration of $HBrO_2$ and Br^- ions, respectively, while τ, a and b represent the reaction parameters. The value of τ is generally set at $\tau \ll 1$ since the reaction rate of $HBrO_2$ ions is much faster than that of Br^- ions. The nullclines of the Oregonator where $d[x_1]/dt = 0$ and $d[x_2]/dt = 0$ are given by

$$[x_2] = \frac{[x_1]([x_1]+b)(1-[x_1])}{a([x_1]-b)}, \quad (\equiv l_1) \tag{5}$$

$$[x_2] = [x_1]. \quad (\equiv l_2) \tag{6}$$

The cross point of these two nullclines (l_1 and l_2) represents the fixed point of the Oregonator.

Figure 1 plots the nullcline and trajectories of the Oregonator with typical parameter-values ($\tau = 10^{-2}$ and $b = 0.02$). The value of parameter a is set at 1 [Fig. 1(a)] and 3 [Fig. 1(b)]. Depending on the position of the fixed point, the Oregonator exhibits oscillatory or excitatory behavior. When $a = 1$, the fixed point is located on nullcline l_1 at which $d[x_2]/d[x_1] > 0$. In this case, the Oregonator exhibits limit-cycle oscillations [Fig. 1(a)]. The oscillations represent periodic oxidation-reduction phenomena in the BZ reaction. On the other hand, the fixed point is located on nullcline l_1 at which $d[x_2]/d[x_1] < 0$ when $a = 3$. Under these conditions, the Oregonator exhibits excitatory behavior [Fig. 1(b)] and is stable atthe fixed point as long as an external stimulus is not applied.

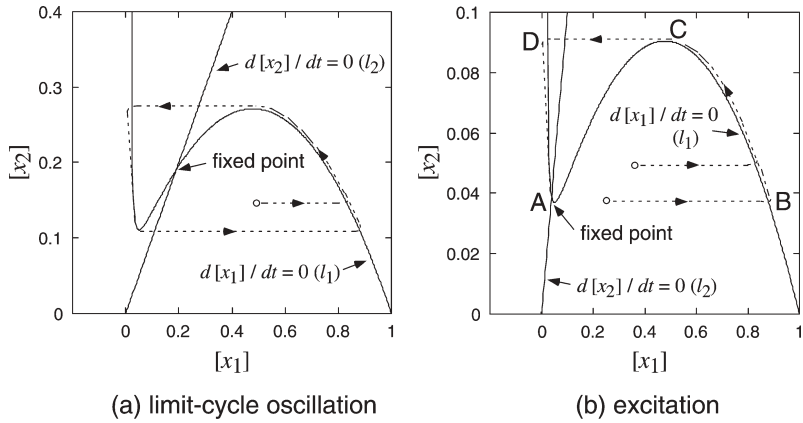

FIGURE 1
Nullclines and trajectories of Oregonator operating in (a) oscillatory mode ($a = 1$) and (b) excitatory mode ($a = 3$).

Three circulative states are introduced in the Oregonator according to the oscillation phase; i.e., inactive (A), active (B → C), and refractory periods (D → A), as labelled in Fig. 1(b). The inactive, active, and refractory states represent a depletion in Br^- ions, an autocatalytic increase in $HBrO_2$ ions (oxidation of the catalyzer), and a depletion in Br^- ions (reduction of the catalyzer), respectively. When the Oregonator is inactive, it is easily activated (A → B) by external stimuli. Then, it turns to the refractory state (C → D). During the refractory state, the Oregonator cannot be activated even if external stimuli are applied.

It should be noted that Eqs. (1) to (4) represent the time difference in chemical species at a *point* in the reaction space. If the spatial distribution of the chemical species is not uniform, the species will diffuse according to the gradient of the concentration of the species. Such a diffusive-reaction system with multiple chemical species is referred to as a *reaction-diffusion* (RD) *system*, and is described by a set of partial differential equations as

$$\frac{\partial [x_i](\mathbf{r},t)}{\partial t} = D_i \nabla^2 [x_i] + f_i([x_1],[x_2],\ldots,[x_N]), \tag{7}$$

where $\mathbf{r}$ represents the space, ∇^2 the spatial Laplacian, and D_i the diffusion constant. A two variable RD system on a 2D plane, which is referred to as a basic RD system, is described in terms of Eq. (7) as

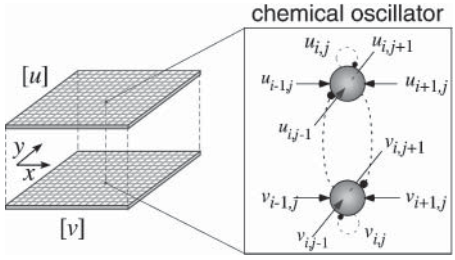

FIGURE 2
Discrete representation of 2D RD system, where each chemical oscillator is locally interconnected. An oscillator located at position (i, j) has two system variables $[u_{i,j}]$ and $[v_{i,j}]$.

$$\frac{\partial[u](x,y,t)}{\partial t} = D_u\left(\frac{\partial^2[u]}{\partial x^2} + \frac{\partial^2[u]}{\partial y^2}\right) + f_u([u],[v]), \tag{8}$$

$$\frac{\partial[v](x,y,t)}{\partial t} = D_v\left(\frac{\partial^2[v]}{\partial x^2} + \frac{\partial^2[v]}{\partial y^2}\right) + f_v([u],[v]), \tag{9}$$

where (x, y) represents the space, and $([u], [v])$ the concentration of two-different chemical species [27].

Figure 2 is a schematic showing an alternative construction to the basic RD system. It consists of a 2D array of chemical oscillators; e.g., Oregonators, where each oscillator is locally interconnected. An oscillator located at position (i, j) has two system variables $[u_{i,j}]$ and $[v_{i,j}]$. The dynamics are defined as

$$\frac{d[u_{i,j}]}{dt} = f_u([u_{i,j}],[v_{i,j}]) + g^u_{i,j}, \tag{10}$$

$$\frac{d[v_{i,j}]}{dt} = f_v([u_{i,j}],[v_{i,j}]) + g^v_{i,j}, \tag{11}$$

where functions f_u and f_v represent the nonlinear chemical interactions between $[u_{i,j}]$ and $[v_{i,j}]$, and where $g^u_{i,j}$ and $g^v_{i,j}$ represent the external inputs to the oscillator. External inputs are applied to an oscillator so that activities $[u_{i,j}]$ and $[v_{i,j}]$ can diffuse throughout the 2D array of oscillators. Such inputs are given by five-point approximation of the Laplacian on the 2D rectangular grid as

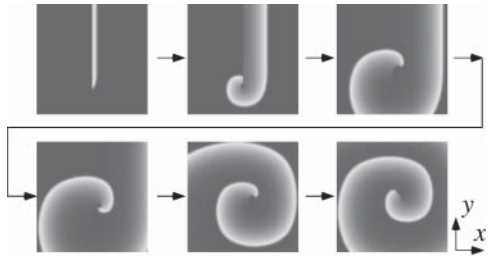

FIGURE 3
Typical numerical results of 2D RD system using Oregonator. Each oscillator was set in the excitatory mode ($a = 3$).

$$g^u_{i,j} = D_u \frac{[u]_{i-1,j} + [u]_{i+1,j} + [u]_{i,j-1} + [u]_{i,j+1} - 4[u]_{i,j}}{h^2},$$

$$g^v_{i,j} = D_v \frac{[v]_{i-1,j} + [v]_{i+1,j} + [v]_{i,j-1} + [v]_{i,j+1} - 4[v]_{i,j}}{h^2},$$

where h represents the distance between neighboring oscillators. The dynamics of a single oscillator [Eqs. (10) and (11)] thus represent the discrete expression of Eqs. (8) and (9). This expression allows us to understand the relation between natural RD systems and the physical hardware structure. Namely, 2D RD phenomena can be imitated on *solid-state medium* (e.g., VLSIs) where numerous hardware oscillators are regularly arranged on VLSIs with diffusive coupling among the local oscillator circuits.

Figure 3 shows numerical solutions to Eqs. (10) and (11) using an Oregonator with typical parameter values. The nonlinear reactive functions $f_u(\cdot)$ and $f_v(\cdot)$ in Eqs. (10) and (11) are replaced with the right sides of Eqs. (3) and (4), respectively, with the transformation of system variables ($[x_1] \to [u_{i,j}]$ and $[x_2] \to [v_{i,j}]$). Each oscillator was set in the excitatory mode ($a = 3$), and the values of the rest of the parameters were $h = 0.01$, $D_u = 5 \times 10^{-4}$, $D_v = 0$, $\tau = 10^{-2}$, and $b = 0.02$. The solution was numerically obtained by solving the ODEs with the fourth-order Runge-Kutta method. At each side of the square reaction-space, the Neumann boundary condition was applied as:

$$\nabla[u] = \nabla[v] = (0,0), \tag{12}$$

where $\nabla[u] = (\partial/\partial x, \partial/\partial y)$; e.g., the values of $[u_{0,j}]$ and $[u_{N+1,j}]$ are treated as those of $[u_{1,j}]$ and $[u_{N,j}]$, respectively. In Fig. 3, the values of $v_{i,j}$ are represented on a grayscale ($v_{i,j} = 0$: black, $v_{i,j} = 1$: white). Several oscillators adjacent to the inactive oscillators were initially set at a refractory state (left side of white bar in Fig. 3). The inactive oscillators adjacent to the white bar were suppressed by the adjacentoscillators in the refractory state (oscillators in white bar). The inactive oscillators then entered an active, inactive, or refractory state, depending on the degree of refractiveness. When the inactive oscillators were in an active or inactive state, the tip of the bar rotated inward, resulting in the generation of spiral patterns that are typically observed in BZ reactions.

3. MODELLING REACTION-DIFFUSION SYSTEM WITH ANALOG CELLULAR-AUTOMATON

A cellular-automaton (CA) is a discrete dynamical system whose behavior is completely specified in terms of finite local interactions [1,29,39], and is thus suitable for VLSI implementation [8,34]. The discrete expression of basic RD models, introduced in Sec. 2, has significant similarity to the CA system [13,36]. First, it consists of a number of identical cells (processors) and local connections between these cells. Second, these cells are regularly arrayed on a 2D rectangular grid. Thus, the basic RD model can be replaced with a CA model by assuming that: i) each cell represents interactions between species $u_{i,j}$ and $v_{i,j}$ at the specific point (i, j), ii) the concentration of chemical species ($[u_{i,j}]$, $[v_{i,j}]$ is represented by the values of system variables in each cell, and iii) local connections between cells are used to diffuse the values of system variables , i.e., the diffusion of chemical species.

3.1 Digital CA model for RD systems

Gerhardt *et al.* proposed a CA model that used a 2D array of digital oscillators (cells) that imitated the Oregonator [17]. The Oregonator was described using continuous system variables, but they introduced discrete system variables and discrete time into the cells. In the model, a cell corresponded to a point in the BZ reaction space; e.g., a 2D BZ reaction was imitated by arranging the cells on a grid. Two types of system variables that represented the concentration of $HBrO_2$ and Br^- ions at position (i, j); i.e., $[u_{i,j}]$ and $[v_{i,j}]$, respectively, were used in the model. Variable

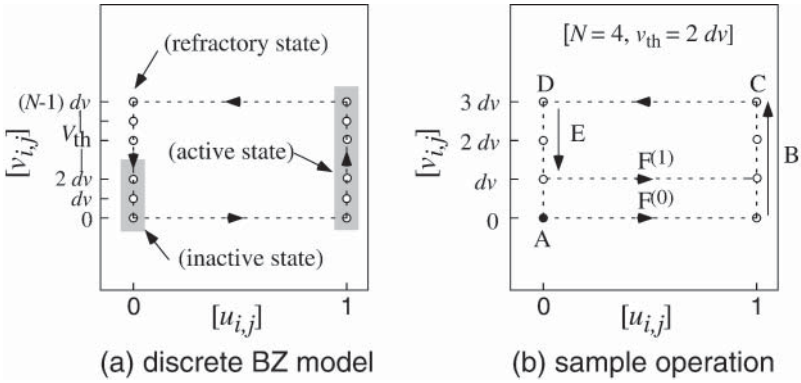

FIGURE 4
State diagram of digital CA for Oregonator. (a) Reaction states are discriminated by values of $[u_{i,j}]$ and $[v_{i,j}]$ and are represented by gray boxes; (b) examples of transition when $N = 4$.

$[u_{i,j}]$ took a binary value, while $[v_{i,j}]$ took multiple values as $n\,dv$, ($dv = 1/N$, $n = 0, 1, \ldots, N-1$).

Figure 4 plots a circulative state-diagram of a single cell. The reaction states are discriminated by the values of $[u_{i,j}]$ and $[v_{i,j}]$ and are represented by the gray boxes in Fig. 4(a). A cell can be activated ($[u_{i,j}] = 0 \rightarrow 1$) only when $[u_{i,j}] = 0$ and $0 \leq [u_{i,j}] \leq v_{\text{th}}$ by collective activations in its neighboring cells [as transition $F^{(0)}$ or $F^{(1)}$ in Fig. 4(b)]. During a refractory state ($[u_{i,j}] = 0$ and $v_{\text{th}} \leq [v_{i,j}] \leq (N-1)dv$), the cellcannot be activated by its neighboring cells. Once the cell is activated, the value of $[v_{i,j}]$ is increased as the discrete time step increases [B in Fig. 4(b)]. When the value of $[v_{i,j}]$ reaches its maximum value $(N-1)dv$ [C in Fig. 4(b)], the cell is deactivated and the value of $[v_{i,j}]$ is decreased as the time step increases [D to A in Fig. 4(b)].

3.2 Analog CA model for BZ reaction

We now introduce an analog cell that is qualitatively equivalent to the Oregonator. Let us consider the following dynamics of a cell:

$$\frac{d[x_1]}{dt} = \frac{1}{\tau}(-[x_1] + f([x_1] - [x_2], \beta_1)), \tag{13}$$

$$\frac{d[x_2]}{dt} = -[x_2] + f([x_1] - \theta, \beta_2), \tag{14}$$

where $f(\cdot)$ represents a sigmoid function defined by

$$f(x,\beta)=\frac{1+\tanh\beta x}{2}. \tag{15}$$

The cell dynamics are designed so that the shape of nullcline and velocity flows ($[\dot{x}_1]$, $[\dot{x}_2]$) are qualitatively equivalent to that of the Oregonator. The cubic nullcline (l_1 in Fig. 1) is approximated by a nullcline of Eq. (13) as

$$[x_2]=[x_1]-\beta_1^{-1}\tanh^{-1}(2[x_1]-1), \quad (\equiv L_1) \tag{16}$$

while the linear nullcline (l_2 in Fig. 1) is approximated by a nullcline of Eq. (14) as

$$[x_2]=f([x_1]-\theta,\beta_2). \quad (\equiv L_2) \tag{17}$$

An analog cell, whose dynamics are described by Eqs. (13) and (14), is very suitable for implementation in analog VLSIs because the sigmoid function can easily be implemented on VLSIs by using differential-pair circuits.

The cell exhibits qualitatively equivalent behavior to the Oregonator, as we can see from Fig. 5. The values of the parameters are $\tau^{-1}=10$, $\beta_1=5$ and $\beta_2=10$. When $\theta=0.5$, the fixed point exists on a nullcline

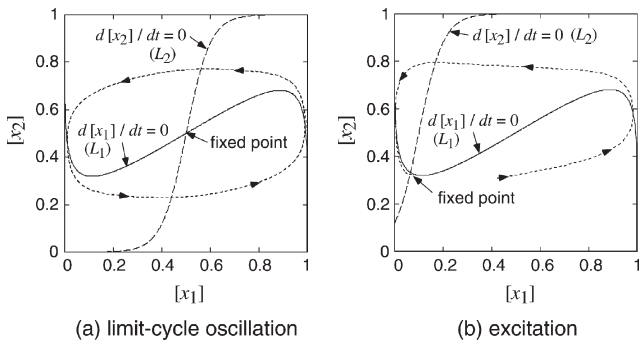

FIGURE 5
Nullclines and trajectories of analog cell operating in (a) oscillatory mode ($\theta=0.5$) and (b) excitatory mode ($\theta=0.14$).

[Eq. (16)] where $d[x_2]/d[x_1] > 0$, and the system exhibits limit-cycle oscillations [Fig. 5(a)]. The system exhibits excitatory behavior [Fig. 5(b)], on the other hand, when the fixed point exists on a nullcline [Eq. (17)] where $d[x_2]/d[x_1] < 0$ [Fig. 5(b)].

Let us introduce cell dynamics into the basic RD model for the purpose of constructing a 2D CA system. The dynamics of the CA are obtained by substituting the right terms of Eqs. (13) and (14) for the nonlinear reactive functions $f_u(\cdot)$ and $f_v(\cdot)$ in Eqs. (10) and (11), and by transforming the system variables ($[x_1] \to [u_{i,j}]$ and $[x_2] \to [v_{i,j}]$). The resulting dynamics of an analog cell are

$$\frac{d[u_{i,j}]}{dt} = \frac{1}{\tau}(-[u_{i,j}] + f([u_{i,j}] - [v_{i,j}], \beta_1)) + g^u_{i,j}, \tag{18}$$

$$\frac{d[v_{i,j}]}{dt} = -[v_{i,j}] + f([u_{i,j}] - \theta, \beta_2) + g^v_{i,j}, \tag{19}$$

where $g^u_{i,j}$ and $g^v_{i,j}$ represent external inputs to the cell (interactions between cell and neighboring cells) defined in Sec. 2.

Figure 6 shows the spatiotemporal activities of the analog CA [Eqs. (18) and (19)] with 50×50 cells ($\beta_1 = 5$, $\beta_2 = 10$, $h = 0.01$ and $D_v = 0$) where the values of $v_{i,j}$ are represented on a grayscale ($v_{i,j} = 0$: black, $v_{i,j} = 1$: white). The Neumann boundary condition was applied at the side of the square reaction-space. When $\tau^{-1} = 10^2$ and $\theta = 0.14$, at which the cell exhibits excitatory behavior, the 2D CA system produced spiral patterns [Fig. 6(a)], as can be observed in the basic RD system with the Oregonators (Fig. 3). In the simulation, diffusion coefficient D_u was set at 5×10^{-4}, and the initial states of cells were set at the same states as in Fig. 3. The results indicate that the analog CA is qualitatively equivalent to the basic RD system with the Oregonators since the excitatory properties of the analog cells are inherently the same as those of the Oregonator.

Figure 6(b) shows the dynamic behaviors of the analog CA with $D_u = 10^{-3}$ and $\theta = 0.5$, at which the cell exhibits oscillatory behavior. The initial values of the cells were randomly chosen as $[u_{i,j}] = \text{RAND}[0,1]$ and $[v_{i,j}] = \text{RAND}[0,1]$, where RAND[0,1] represents random real numbers between 0 and 1. The CA produced 2D phase-lagged stable synchronous patterns called *modelock*, due to weak coupling between the neighboring cells. When $D_u > 10^{-3}$, all cells exhibited synchronous oscillation (no spatial patterns were produced).

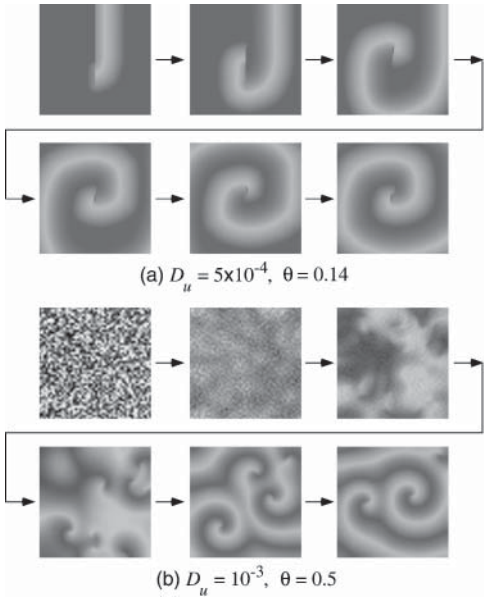

FIGURE 6
Numerical results for RD system with (a) excitatory cells and (b) oscillatory cells.

4. CMOS IMPLEMENTATION OF ANALOG CA MODEL FOR BZ REACTION

This section describes the analog cell and discusses its great suitability for analog VLSIs, as discussed in the previous section. The resulting cell circuit consists of just a capacitor and two operational-transconductance amplifiers (OTAs). Consequently, the circuit can easily be implemented on silicon VLSIs using conventional CMOS technology.

When the rate constant of Eq. (13) is much larger than that of Eq. (14), the differential term of Eq. (13) can be neglected ($\tau \ll 1$), as explained in Sec. 2. On the other hand, Eq. (14) with $\beta_2 \to \infty$ forces the values of variable $[x_2]$ to be 0 when $[x_1] \leq \theta$, and while $[x_2] \to 1$ when $[x_1] > \theta$. Thus, if variable $[x_2]$ is forced to have a value within range [0:1], the temporal difference in Eq. (14) can approximately be represented by binary values. Consequently, one can obtain a new dynamical equation from Eqs. (13) and (14) as

$$[x_1] = f([x_1] - [x_2], \beta_1) \tag{20}$$

$$\frac{d[x_2]}{dt} = \begin{cases} w & (\text{if } [x_1] > \theta) \\ -w & (\text{else}) \end{cases} \tag{21}$$

where w represents a positive, small constant. We designed an analog cell circuit that could easily be implemented on VLSIs, based on these equations.

The cell circuit used standard OTAs. The construction of a single OTA is represented by the dashed ellipse in Fig. 7. It transduces differential input voltages ($V_1 - V_2$) to current [$-I_{ref}$: I_{ref}]. When all the transistors are operated in their subthreshold region, the output current is given by

$$I_{out} = I_{ref} \tanh \frac{\kappa(V_1 - V_2)}{2V_T}, \tag{22}$$

where κ represents the effectiveness of the gate potential and $V_T \equiv \kappa T/q = 26$ mV at room temperature (κ is Boltzmann's constant, T the temperature, and q the charge of an electron) [22]. This OTA can also be used in the open-circuit mode as a differential-voltage amplifier. Its open-circuit voltage gain at $V_1 \approx V_2$ is given by

$$A = \frac{\kappa V_0}{2V_T}, \tag{23}$$

where V_0 represents the early voltage of output transistors (M1 and M2). Since the output voltage of the OTA is saturated to its supply voltage VDD (or VSS) when $V_1 > V_2$ (or $V_1 > V_2$), its input-output characteristics are approximately represented by a piecewise linear function as

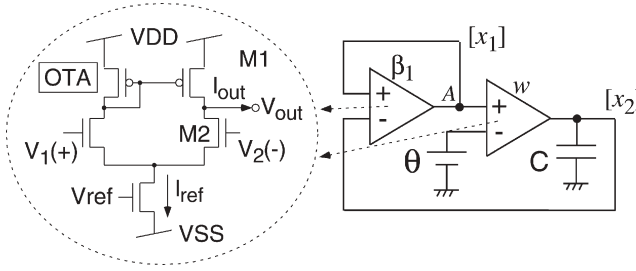

FIGURE 7
Analog cell circuit consisting of single capacitor and two operational-transconductance amplifiers (OTAs).

$$V_{\text{out}}(x) \equiv F(x) = \begin{cases} \text{VDD} & (x \gg 0) \\ A\,x & (x \approx 0) \\ \text{VSS} & (x \ll 0), \end{cases} \tag{24}$$

where $x \equiv V_1 - V_2$.

Figure 7 is a circuit diagram for the analog cell. It consists of a single capacitor and two OTAs labeled β_1 and w. From Eqs. (22) and (24), the dynamics of the cell circuit are represented by

$$[x_1] = F([x_1] - [x_2]), \tag{25}$$

$$C\frac{d[x_2]}{dt} = I_{\text{ref}} \tanh \frac{\kappa([x_1] - \theta)}{2V_T}, \tag{26}$$

where F is the piecewise linear function defined in Eq. (24). In the figure, OTA β_1 serves as the function of Eq. (25), while capacitor C and OTA w receiving voltage θ produce the dynamics for Eq. (26). Equation (26) can further be simplified as

$$C\frac{d[x_2]}{dt} = \begin{cases} I_{\text{ref}} & ([x_1] > \theta) \\ -I_{\text{ref}} & (\text{else}) \end{cases} \tag{27}$$

when $\kappa/V_T \gg 1$. The output current of OTA w becomes 0 when the voltage of output node $[x_2]$ equals the supply voltage (VDD or VSS). The value of $[x_2]$ is thus restricted within range [VDD:VSS]. Note that Eqs. (25) and (27) are qualitatively equivalent to (20) and (21), respectively.

5. RESULTS

5.1 Circuit Simulations with SPICE

Figure 8 shows the layout of a cell circuit obeying the MOSIS 1.5-μm standard n-well CMOS rule. This device consists of four blocks; i.e., OTA β_1, OTA w, MOS capacitor C, and the output driver (inverter). The size of the analog cell was 70×70 μm^2. The supply voltages of OTA β_1 are labeled as VDD2 and VSS2, while that of OTA w and the driver are labeled as VDD1 and VSS1. The well and substrate are common to all blocks, and are connected to VDD1 and VSS1, respectively. The following results were obtained from extracted circuits from the device layout (Fig. 8) with actual parasitic capacitances. A MOSIS 1.5-μm CMOS

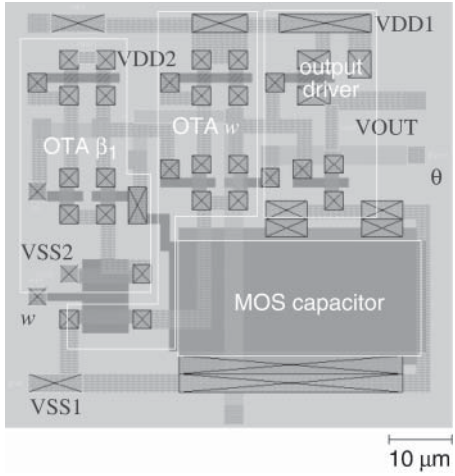

FIGURE 8
Layout for analog cell designed with 1.5-μm CMOS rule (cell size: 70×70 μm^2).

technology file with a transistor model of BSIM3 (level 8) and ngspice (rework-14) were used to evaluate the circuit with an actual device layout. The size of the MOS transistors was set at $W/L = 5\lambda/10\lambda$ for transistors providing source currents of OTAs and $W/L = 5\lambda/2\lambda$ to the others ($\lambda = 0.8$ μm). Capacitor C was replaced with an nMOS capacitor (lower-right rectangle in Fig. 8).

Figure 9 plots the nullclines of the cell circuit. The supply voltages VDD1, VDD2, VSS1, and VSS2 were set at 5 V, 4 V, GND, and 0.5 V,

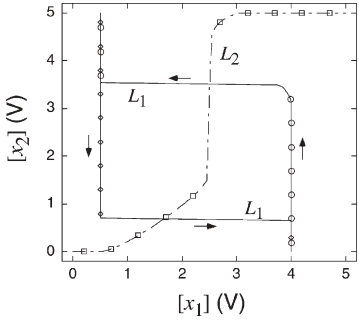

FIGURE 9
Numerically obtained nullclines of analog cell circuit.

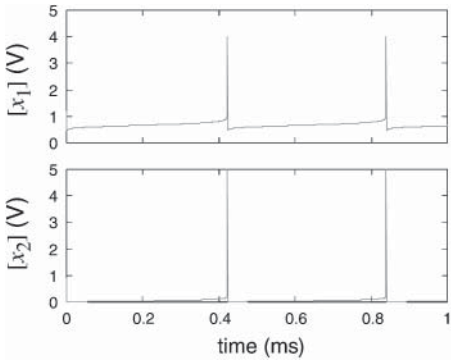

FIGURE 10
Time course for cell circuit's system variables ([x_1], [x_2]).

respectively. Bias voltage V_{ref} was set at 2 V, while threshold θ was set at 2.5 V so that the circuit would exhibit oscillatory behavior. In the figure, hysteresis curve L_1 representing the inverse "N" characteristic corresponds to the nullcline of Eq. (16), while L_2 represents the nullcline of Eq. (17). Time courses for [x_1] and [x_2] are plotted in Fig. 10. Stiff oscillations were obtained as observed in a typical BZ reaction. The stiffness and frequency of the oscillations can be controlled with the reference voltages of the OTAs (V_{ref} in Fig. 7). In the simulation, the reference voltage for OTA w_1 was the same as that for OTA w.

According to Eqs. (25) to (27), [x_2] should only increase if [x_1] is greater than threshold θ. In addition, Eq. (27) indicates that the decreasing rate of [x_2] should be equal to the increasing rate. This implies a triangular wave oscillation in [x_2] and a square wave oscillation in [x_1]. However, the results clearly show that [x_2] was increasing while [x_1] was equal to $0.5\ \text{V} < \theta$. In the circuit, OTA w cannot produce ideal sigmoid-type nullcline L_2, as seen in Fig. 9, due to the unsaturated operation of the source nMOS transistor. Therefore, [x_1] and [x_2] change very slowly when [x_2] is lower than the threshold voltage of an nMOS transistor (V_{th}) and $[x_1] < \theta$, compared with $[x_2] > V_{th}$ and $[x_1] > \theta$. This operation generates the stiff oscillation rather than triangular and square wave oscillations. Note that if full-range OTAs had been used instead of the 5-transistor OTA employed here, such triangular and square oscillations would have been obtained.

Figure 11 plots the synchronizing phenomena for three cell circuits. These cell circuits were locally connected by pass transistors, instead of

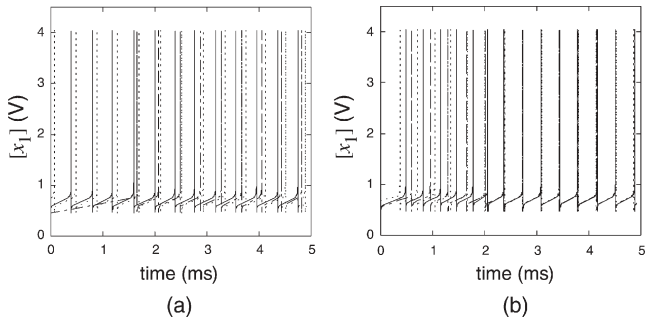

FIGURE 11
Time course for three analog cells coupled by pass transistors with (a) very weak and (b) weak connections.

linear resistors, because if the qualitative behaviors of the system had not been changed by nonlinearity, theywould have reduced circuit size significantly. The connection strength was thus controlled by the common gate voltage (V_g) of these transistors. In the simulation, the bias condition was the same as in the previous experiments, and the output node $[x_1]$ of each cell was connected to that of two neighbors with minimum-size nMOS (pass) transistors. Output node $[x_2]$ was not connected anywhere. When $V_g = 0$, each circuit oscillated independently [Fig. 11(a)]. As $V_g \rightarrow$ VDD, these circuits tended to exhibit synchronizing oscillatory behaviors. Fig. 11(b) plots gradual synchronizing behavior ($V_g = 0.9$ V). Initially, the oscillators were not synchronized. After $t = 2$ ms, they were.

A 2D array of cell circuits (8×8 cells) was designed, as we can see from Fig. 12. The size of array was 970×1050 μm^2 using the 1.5-μm CMOS design rule. The cell circuits were regularly arrayed on a 2D rectangular grid. Each cell was locally connected to its four neighbors with four pass transistors (nonlinear resistors). Figure 13 has snapshots at $t = n\Delta t$ ($\Delta t = 20$ μs) of spatiotemporal outputs of the 2D array. In the simulation, V_g was set at 1.5 V with an open boundary condition. The rest of the parameters were the same as in the previous experiments. In the photographs, voltages $[x_1]_{i,j}$ are represented on a grayscale ($v_{i,j} = 0$: black, $v_{i,j} = 4$ V: white). The initial values of the cell circuits were randomly chosen as $[u_{i,j}]$ = RAND[0.5V, 4V] and $[v_{i,j}]$ = RAND[0V, 5V]. The distribution became almost uniform at $t = 5\Delta t$. During $t = 5\Delta t \rightarrow 50\Delta t$, the cell circuit located at the bottom-right corner was oscillating by chance. Depending on the initial conditions, the position of a cell such as this that

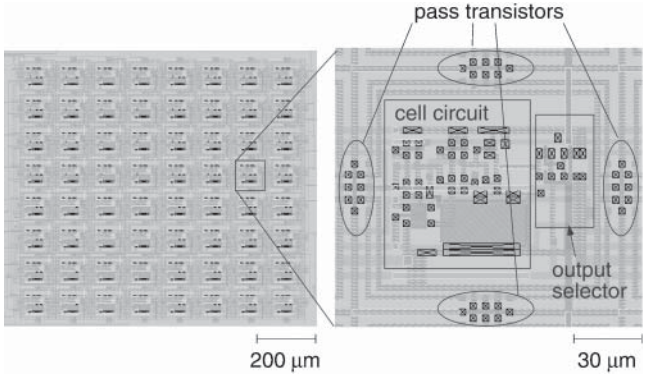

FIGURE 12
Layout of 8 × 8 analog cells designed with 1.5-μm CMOS rule (array size: 970 × 1050 μm^2).

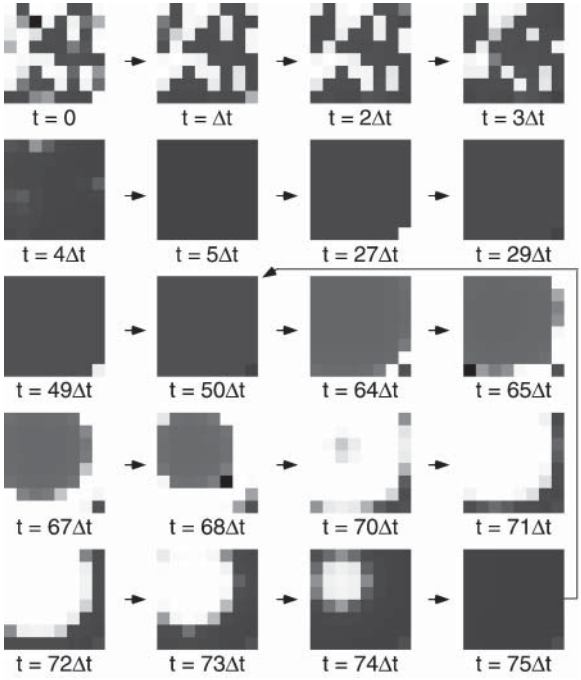

FIGURE 13
Generation of active traveling waves in 2D RD chip.

survives will be changed. The surviving cell's neighbors were stimulated through pass transistors. Consequently, theneighbors were excited at $t = 64\Delta t$, and chain excitation was observed during $t = 65\Delta t \rightarrow 75\Delta t$. After $t = 75\Delta t$, the "seed" cell at the bottom-right corner was still oscillating, which induced subsequent chain excitation. Consequently, this array produced 2D phase-lagged stable synchronous patterns. When $V_g > 1$ V, all cells exhibited synchronous oscillations (no spatial patterns were produced). The results indicate that although a simplified cell circuit and nonlinear resistors (pass transistors) were used, the analog system is qualitatively equivalent to the basic RD system with the Oregonators since the excitatory properties of the analog cells are inherently the same as those of the Oregonator.

5.2 Experimental Results with Fabricated RD Chip

A prototype RD chip was fabricated with the 1.5-μm CMOS process (MOSIS, vendor: AMIS). Figure 14 is a micrograph of the RD chip that includes an array of cell circuits (example in Fig. 12). An array of 8×8 cell circuits was implemented on a 2.3×2.3 mm^2 die.

Figure 15 plots experimental results for a reaction circuit. The upper and lower graphs plot time courses of voltage $[x_1]$ and $[x_2]$ in the circuit. The supply voltages of an OTA of β_1 was set at VDD = 4 V and VSS = 0.5 V, while that of the remaining OTA (ω) was set at VDD = 5 V and VSS = GND. Threshold θ was set at 2.5 V so that the circuit exhibited oscillatory behaviors. As expected, the circuit exhibited the same qualitative behaviors as in the simulation results (Fig. 10); i.e.,stiff nonlinear oscillations. In the experiment, V_{ref} was set just above the threshold voltage of an nMOS transistor; i.e., the OTA was driven by a current of $O(10^{-6})$ A.

The operations of the 8×8 reaction cell array were recorded with the following readout circuitry. Each cell in the chip was located beneath each wire crossing row and column buses, and was connected to a common-output wire through a transfer gate. The gate connects the cell's output to the common wire when both the row and column buses are active. The cell's output $[x_2]$ is amplified by an inverter (output driver) in the prototype chip. Thus a cell's quantized output appeared on the common output wire when the cell was selected by activating the corresponding row and column buses simultaneously. One could obtain a binary stream from the common output wire by selecting each cell

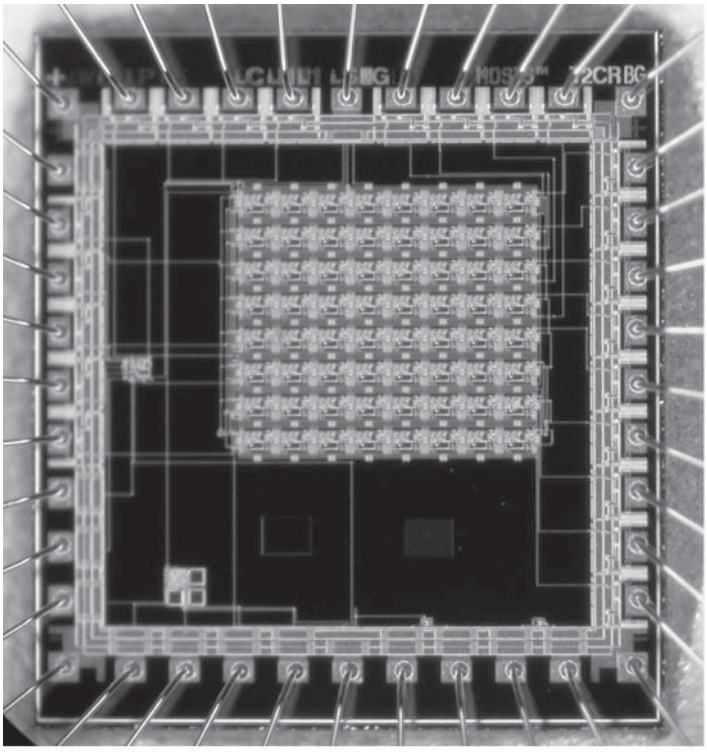

FIGURE 14
Micrograph of fabricated RD chip.

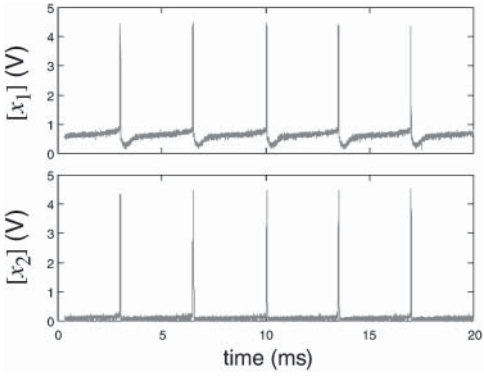

FIGURE 15
Experimental results for reaction circuit operating in its oscillatory mode.

sequentially. Using a conventional displaying technique, the binary-stream was reconstructed on a 2-D display. Figures 16 to 18 present the recorded results. Each white dot represents an inactive cell where $[x_2] < \mathrm{VDD}/2$. In the experiment, V_{ref} was set at the threshold voltage of an nMOS transistor; i.e., the OTAs were driven by the subthreshold current, so that "very-slow" spatiotemporal activities could be observed visually. The remaining parameters were the same as in the experiments in Fig. 15. When V_g (common gate-voltage of pass transistors) was set at 0, each cell oscillated independently (Fig. 16). Snapshots were taken at intervals of 200 ms. The collective activities of cell clusters were observed by increasing V_g. Figure 17 presents an example where some spiral (modelock) patternsof cell clusters were observed ($V_g = 0.8$ V). Snapshots were taken with at intervals of 100 ms. The active-cell clusters and cores of the spirals are superimposed with the figure by white curves and white circles, respectively. Although observing"beautiful" spirals as in Fig. 6 is difficult because of the small number of cells, the appearance and disappearance of small sections of spiral waves were successfully observed. Under strong lateral connections ($V_g = 1.2$ V), large cluster of cells were synchronized, as we can see in Fig. 18. Due to mismatches of fabricated devices, the cells were not synchronized even when $V_g > 1.2$ V.

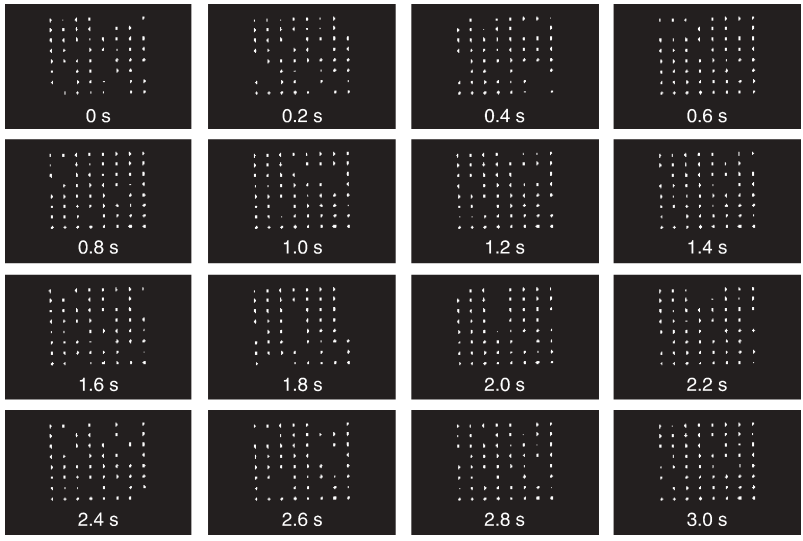

FIGURE 16
Spatiotemporal patterns on the fabricated RD chip (no lateral connections between cells).

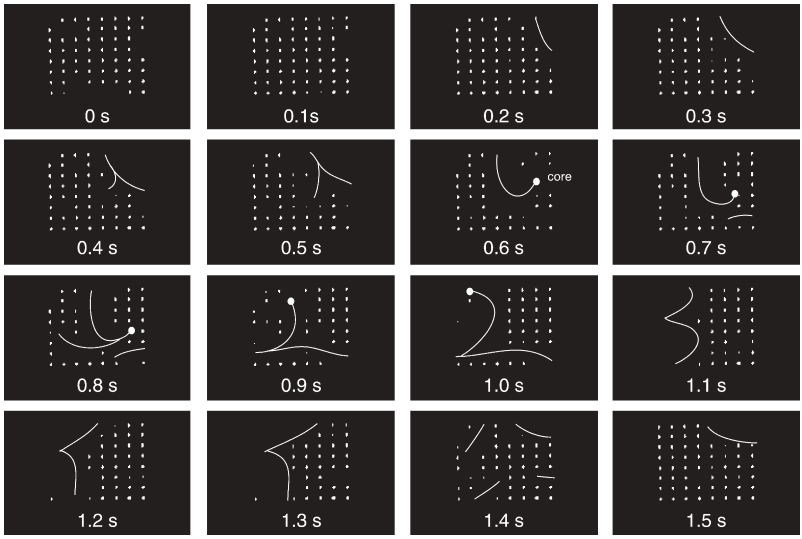

FIGURE 17
Spiral patterns on RD chip (weak connections between cells).

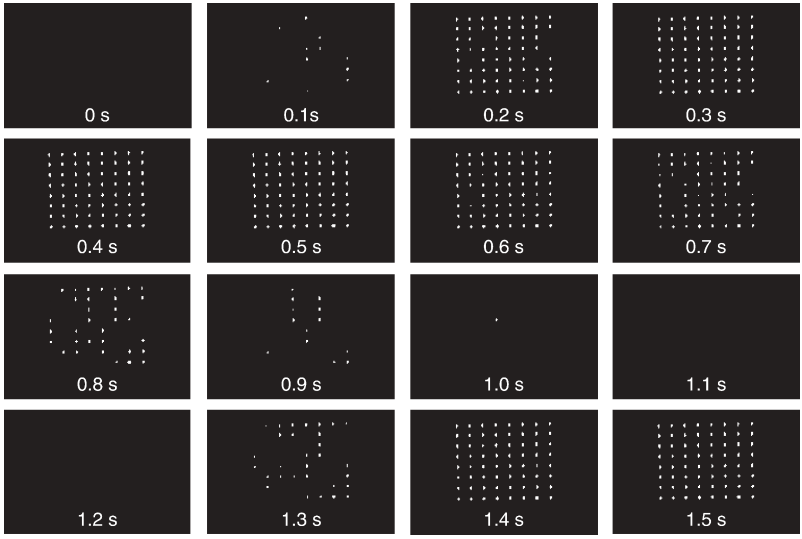

FIGURE 18
Synchronization of cells on RD chip (strong connections).

These results indicate the expected operations of the RD chip. The next challenge is to develop RD chips with a more microscopic process because a large number of reaction cells must be implemented on a chip to observe complex (BZ-like) patterns. Furthermore, at this stage, each reaction cell should have optical sensors for parallel inputs. In fact, the optical input of data-information was already used at the beginning of RD research [21]. This was proven to be particularly important in experiments on image processing in BZ-medium-based computing devices.

6. SUMMARY

Silicon devices that imitate the autocatalytic and dissipative phenomena of reaction-diffusion (RD) systems were introduced. Numerical simulations and experimental results revealed that an RD device could successfully produce concentric and spiral waves in the same way as natural RD systems. These results encouraged us to develop new applications based on natural RD phenomena using hardware RD devices.

RD devices and circuits are useful not only for hardware RD systems but also for constructing modern neuro-chips. The excitatory and oscillatory behaviors of an RD device and circuit are very similar to actual neurons that produce sequences of identically shaped pulses in time, called *spikes*. Recently, Fukai [1996] demonstrated that an inhibitory network of spiking neurons achieves robust and efficient neural competition on the basis of a novel timing mechanism of neural activity. A network with such a timing mechanism may provide an appropriate platform to develop analog VLSI circuits and could overcome problems with analog devices, namely their lack of precision and reproducibility.

Acknowledgement

The authors wish to thank Professor Andrew Adamatzky (University of the West of England) for most valuable discussions and suggestions during the research. This study was also supported by a grant entitled "Analog Reaction-Diffusion Chip: The Developmentof Functional LSIs Recovering Fingerprint Images" in 2000 from the New Energy and Industrial Technology Development Organization (NEDO) of Japan.

REFERENCES

[1] Adamatzky, A. (1994). *Identification of Cellular Automata*. Taylor & Francis, London.

[2] Adamatzky, A.(2001). *Computing in Nonlinear Media & Automata Collectives*. Institute of Physics Publishing, Bristol.

[3] Adamatzky, A. and De Lacy Costello, B.P.J. (2002a). Collision-free path planning in the Belousov-Zhabotinsky medium assisted by a cellular automaton. *Die Naturwissenschaften, 89*, 474–478.

[4] Adamatzky, A. and De Lacy Costello, B.P.J. (2002b). Experimental logical gates in a reaction-diffusion medium: The XOR gate & beyond. *Physical Review E, 66*, 046112.

[5] Adamatzky, A. and De Lacy Costello, B.P.J. (2003). On some limitations of reaction-diffusion computers in relation to Voronoi diagram and its inversion. *Physical Letter A, 309*, 397–406.

[6] Adamatzky, A., De Lacy Costello, B., Melhuish, C., and Ratcliffe, N. (2003). Experimental reaction-diffusion chemical processors for robot path planning. *Journal of Intelligent & Robotic Systems, 37*, 233–249.

[7] Agladze, K., Magome, N., Aliev, R., Yamaguchi, T., and Yoshikawa, K. (1997). Finding the optimal path with the aid of chemical wave. *Physica D, 106*, 247–254.

[8] Asai, T., Sunayama, T., Amemiya, Y., and Ikebe, M. (2001). A *v*MOS vision chip based on the cellular-automaton processing. *Japanese Journal of Applied Physics, 40*(4B), 2585–2592.

[9] Asai, T., Nishimiya Y., and Amemiya, Y. (2002). A CMOS reaction-diffusion circuit based on cellular-automaton processing emulating the Belousov-Zhabotinsky reaction. *IEICE Transactions on Fundamentals, E85-A*(6), 2093–2096.

[10] Asai T., Adamatzky, A., and Amemiya, Y. (2004). Towards reaction-diffusion computing devices based on minority-carrier transport in semiconductors. *Chaos, Solitons & Fractals, 20*(4), 863–876.

[11] Blittersdorf, R., Müller, J., and Schneider, F.M. (1995). Chemical visualization of boolean functions: a simple chemical computer. *Journal of Chemical Education, 72*, 760–763.

[12] Conrad, M. & Zauner, K.P. (2000). Molecular computing with artificial neurons. *Communications of the Korea Information Science Society, 18*(8), 78–89.

[13] Crounse, R.K., Chua, O.L., Thiran P. and Setti G. (1996). Characterization and Dynamics in Cellular Neural Networks. *International Journal of Bifurcation & Chaos, 6*, 1703–1724.

[14] Daikoku, T., Asai, T., and Amemiya, Y. (2002). *An analog CMOS circuit implementing Turing's reaction-diffusion model*, in *Proceedings of the 2002 International Symposium on Nonlinear Theory & its Applications*, pp. 809–812.

[15] Field, J.R. and Burger, M. (1985). *Oscillations and travelling waves in chemical systems*. John Wiley & Sons, Inc.: New York.

[16] Fukai, T. (1996). Competition in the temporal domain among neural activities phase-locked to subthreshold oscillations. *Biological Cybernetics, 75*, 453–461.

[17] Gerhardt, M., Schuster, H., and Tyson, J.J. (1990). A cellular automaton model of excitable media. *Physica D, 46*, 392–415.

[18] Hjelmfelt, A. and Ross, J. (1993). Mass-coupled chemical systems with computational properties. *Journal of Physical Chemistry, 97*, 7988–7992.

[19] Hjelmfelt, A. and Ross, J. (1995). Implementation of logic functions and computations by chemical kinetics. *Physica D, 84*, 180–193.

[20] Hjelmfelt, A., Schneider, F.W., and Ross, J. (1993). Pattern recognition in coupled chemical kinetic systems. *Science, 260*, 335–337.

[21] Kuhnert, L., Agladze, K.L., and Krinsky, V.I. (1989). Image processing using light-sensitive chemical waves. *Nature, 337*, 244–247.

[22] Liu, C.S., Kramer, J, Indiveri, G., Delbrück, T., and Douglas, R. (2002). *Analog VLSI: Circuits and Principles*. The MIT Press, Cambridge, MA.

[23] Müller, C.S. and Keener, P.J. (1995). Spiral Wave Dynamics in *Chemical waves and patterns*, eds. Kapral, R. & Showalter, K. (Kluwer Academic Publishers, Boston) pp. 57–92.

[24] Motoike, I. and Yoshikawa, K. (1999). Information operations with an excitable field. *Physical Review E, 59*, 5354–5360.

[25] Motoike, N.I., Yoshikawa, K., Ighuchi, Y., and Nakata, S. (2001). Real-Time Memory on an Excitable Field. *Physical Review E, 63*, 036220.

[26] Motoike, N.I. and Yoshikawa, K. (2003). Information operations with multiple pulses on an excitable field. *Chaos, Solitons & Fractals, 17*, 455–461.

[27] Nicolis, G. and Prigogine I. (1977). *Self-organization in Nonequilibrium Systems — From Dissipative Structures to Order through Fluctuations*. John Wiley & Sons, Inc., New York, NY.

[28] Oya, T., Ueno, T., Asai, T., and Amemiya, Y. (2003). *Reaction-diffusion systems using single-electron oscillators*, in *Abstract of 2003 Silicon Nanoelectronics Workshop*, pp. 82–83.

[29] Preston K.J. and Duff, BJ.M. (1984). *Modern Cellular Automata: Theory & Applications* (Plenum Press, New York).

[30] Rambidi, N.G. (1998). Neural network devices based on reaction-diffusion media: an approach to artificial retina. *Supramolecular Science, 5*, 765–767.

[31] Rambidi, N.G. and Yakovenchuk, D. (2001). Chemical reaction-diffusion implementation of finding the shortest paths in a labyrinth. *Physical Review, E63*, 0266071–0266076.

[32] Rambidi, N.G., Shamayaev, K.E., and Peshkov, G.Y. (2002). Image processing using light-sensitive chemical waves. *Physical Letter A, 298*, 375–382.

[33] Steinbock, O., Tóth, A., and Showalter, K. (1995). Navigating complex labyrinths: optimal paths from chemical waves. *Science*, 868–871.

[34] Sunayama, T., Ikebe, M., Asai, T., and Amemiya, Y. (2000). Cellular *v*MOS circuits performing edge detection with difference-of-Gaussian Filters. *Japanese Journal of Applied Physics, 39*(4B), 399–407.

[35] Tanaka, H. and Hasegawa, A. (2002). Modelock avoiding synchronization method. *Electronics Letters, 38*(4), 186–187.

[36] Thiran, P., Crounse, R.K, Chua, O.L., and Hasler, M. (1995). Pattern formation Properties of Autonomous Cellular Neural Networks. *IEEE Transactions on Circuits & Systems, Part I, 42*, 757–774.

[37] Tóth, Á., Gáspár, V., and Showalter, K. (1994). Propagation of Chemical Waves through Capillary Tubes. *Journal of Physical Chemistry, 98*, 522–531.

[38] Tóth, A. and Showalter, K. (1995). Logic gates in excitable media. *Journal of Physical Chemistry, 103*, 2058–2066.

[39] Toffoli, T. and Margolus, N. (1987). *Cellular Automata Machines*, MIT Press, Cambridge.

[40] Zauner, K.P. and Conrad, M. (2001). Molecular approach to informal computing. *Soft Computing, 5*, 39–44.